The Development Mechanism for Tibetan Plateau Warm Vortices

BIN WANG*

Geophysical Fluid Dynamics Program, Princeton University, Princeton, NJ 08542

(Manuscript received 10 November 1986, in final form 17 April 1987)

ABSTRACT

The low-level cyclonic vortices which form over the Tibetan Plateau in the summer monsoon season are major rain-producing systems and have the potential to trigger cyclogenesis on the lee side when they move off the plateau. Two cases of the plateau vortices which occurred in July 1979 are studied. The characteristics of the vertical structure in their developing stage, and the circulation conditions favorable for the eastward movement in the mature stage are diagnosed and presented by use of FGGE IIIb datasets. Numerical simulations with real data were performed using the GFDL limited-area mesoscale simulation model. Results suggest that the latent heating is an essential driving force for the development of the vortices studied here.

The analysis of a continuous CISK model with a basic state resembling that actually observed over the summer plateau shows that the predicted unstable mode has a preferred scale, growth rate and vertical structure, all of which are qualitatively comparable to observations. The instability in the plateau environment is mainly attributed to 1) the relatively shallow vertical extent of heating located in the upper troposphere in which the heat capacity of the air column per unit surface area is relatively small; 2) the dramatic reduction of the static stability due to surface sensible heat flux; and 3) the significant increase of moisture content in the plateau boundary layer due to surface evaporation and monsoon transport of water vapor. Most of these favorable conditions are referred to as the dynamic and thermal effects of the elevated plateau terrain. In this sense, the development of the plateau vortices during the rainy season may be regarded as resulting from the interaction between the large-scale circulation and the plateau topographic effects and from the release of convective latent heat.

1. Introduction

During the rainy season of the Tibetan (Qinghai-Xizang) Plateau (June, July and August), the planetary boundary layer over the interior region of the plateau is populated by mesoscale shallow cyclonic vortices with a typical horizontal dimension of several hundred kilometers. They are called Tibetan Plateau low-level vortices (Tao and Ding, 1981), or Tibetan Plateau monsoon depressions (Luo and Wang, 1984), henceforth referred to simply as the plateau vortices.

It has been difficult to determine the accurate geographical distribution of the origin of the plateau vortices due to the scarcity of observations in the western plateau (the region west of 90°E). During the period May–August 1979, the Qinghai-Xizang (Tibet) Plateau Meteorological Experiment (QXPMEX) was conducted along with MONEX and FGGE. There was a significant increase in the number of the observational stations; four new stations were set up to provide supplementary data during the period. Analyses of the observed data in the summer of 1979 show that the vortices are generated in situ over the main body of the plateau, and frequently occur at the central plateau (a region located between 85° and 95°E). Most of the vortices originate on the western central plateau (between 85° and 9°E), develop in the central-eastern plateau as they normally move eastward, and decay when they approach the lee side of the plateau (Luo and Wang, 1984; Qian et al., 1984a).

The plateau vortices, along with the surface shear line associated with them, are major rain-producing weather systems over the plateau. A small portion of these vortices, under proper synoptic situation, may move eastward off the plateau, triggering low-level cyclogenesis on the lee side and giving rise to severe weather over downstream region (Tao and Ding, 1981; Kuo et al., 1986). There are two questions that are of practical importance and of theoretical interest: What mechanism is responsible for the development of plateau vortices? What makes the vortices migrate out of the plateau region?

One of the prominent synoptic features is that the generation of the plateau vortices are often accompanied by an appreciable amount of *convective* precipitation (on average, 6–11 mm per day; see Lu et al., 1984). That is a clue that condensational latent heating may be an important energy source for the summer plateau vortices. Yet, the question is how the latent heat released in cumulus clouds can be employed to produce a growing subsynoptic disturbance in the

* Present affiliation: Department of Meteorology, University of Hawaii, Honolulu, HI 96822.

summer plateau environment where the moisture content in the boundary layer is only about 1/3 of that over a tropical ocean; in particular, there is a question as to how the thermal and dynamic effects of the Tibetan Plateau affect the development process. Besides, it is not clear whether or not other physical processes, such as the instabilities due to horizontal shear in the lower layer and due to horizontally inhomogeneous sensible heating, play a significant part in the development of the plateau vortices. The diagnostic and dynamical understanding of these systems has been rather limited, because they spend most of their existence over the data-sparse plateau (especially the western plateau).

In section 2, two examples of the plateau vortices which occurred during July 1979 are analyzed using GFDL (Geophysical Fluid Dynamics Laboratory) and ECMWF (European Centre of Medium-range Weather Forecast) FGGE IIIb data. One of them concerns a vortex that later moved off the plateau and induced a warm, heavy rain vortex on the lee side, while the other deals with a vortex that died out on the eastern plateau. The purpose of the analysis is to summarize their characteristic vertical structure and identify environmental synoptic conditions that may be favorable for their eastward movement and maintenance. To reveal the roles convective latent heating and dynamic instability play in the vortex development, controlled numerical experiments are performed and the results are discussed in section 3. The major effort of this paper is focused on the study of the development mechanism. To demonstrate how the organized cumulus latent heating contributes to the growth of a shallow meso-alpha-scale vortex in the summer plateau environment, a continuous CISK (Conditionally Instability of the Second Kind) model developed in a previous paper (Wang, 1987a) is applied to plateau vortex events in section 4. The model-predicted mesoscale CISK disturbance has been shown to be fairly comparable to observed Tibetan Plateau warm vortices as far as the growth rate, typical horizontal scale, and vertical structures are concerned. The theoretical analysis also sheds some light on how thermal and mechanical effects of the elevated Tibetan Plateau establish, through interaction with large-scale circulation, a favorable environment that supports the unstable disturbances.

It should be pointed out that there are basically two types of plateau vortices: warm and cold (Luo, 1979). The warm vortices occur more frequently and produce larger amounts of precipitation than cold ones. The discussion in this paper deals only with the warm vortices.

2. The vortex structure and circulation conditions

Two events of the plateau vortices are selected from the period of July 1979. The first event, designated as case A, describes a plateau vortex which formed on the east-central plateau (92.5°E, 33°N) at 12 UTC 13 July and moved to the east edge of the plateau in the ensuing 24 h (Fig. 1). The second, labeled as case B, presents a low vortex which originated at the middle central plateau (90°E, 32°N) at 12 UTC 27 July and died out 24 h later on the eastern plateau (Fig. 1). The locations of the vortices are determined by using both GFDL and ECMWF/FGGE analyses and are compared with the weather map published by the State Meteorological Administration of the People's Republic of China and with the subjective analyses carried out by Qian et al. (1984a) and Qin and Cui (1984). The comparison indicates that the ECMWF/FGGE analysis is better than the GFDL/FGGE analysis for case A, but that the opposite is true for case B. In this section, the analyses for cases A and B are based on the ECMWF and GFDL FGGE IIIb data, respectively.

a. Synoptic conditions prior to the genesis of the vortices

At 00 (0000) UTC 13 July 1979 (time is given by the two-digit hour, hereafter), 12 h prior to the formation of the vortex in case A, a dominant feature of the 500-mb streamline map (not shown) is the extraordinary development of the western Pacific subtropical high (WPSH), which extends westward all the way to the eastern periphery of the Tibetan Plateau. On the central plateau, the prevailing southwest wind brought moist air from India and the Bay of Bengal to the southeastern and central plateau. A region with weak convergence covered the east-central plateau where the vortex was generated 12 h later. Sounding data (32.5°N,

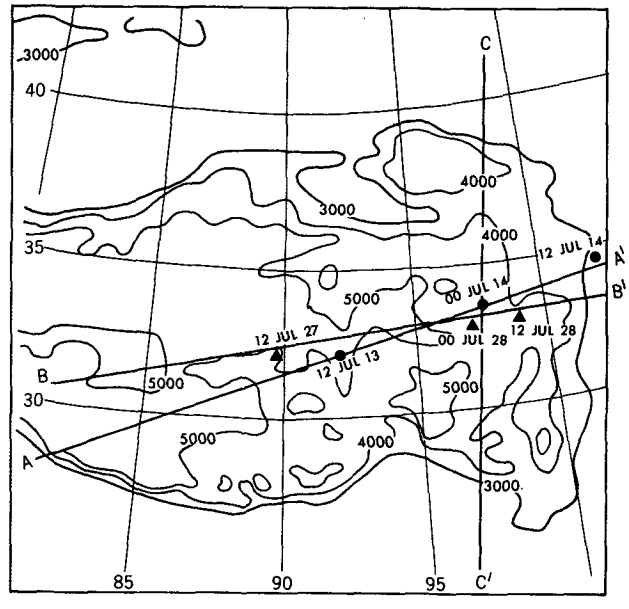

FIG. 1. The map of the model domain, showing the topographic contours and the geographic locations of the vortices during the 13–14 July event (circle) and 27–28 July event (triangle). Line segments AA', BB' and CC' indicate the locations of the vertical cross sections used in Figs. 3, 4, and 7.

92.5°E) (not shown) indicate that the atmosphere was marginally convectively unstable at 00 UTC (local time: 0600) 13 July and became convectively unstable at 12 UTC (local time: 1800). In the vertical cross section along 92.5°E (Fig. 2a), a westerly jet was located north of the plateau at the 12-km level; in the plateau boundary layer, however, both vertical and meridional shears are weak, indicating the lack of local dynamic energy sources.

The synoptic condition leading to the vortex-genesis in case B is similar to that of case A; i.e., (a) the central plateau is a region with weak preexisting convergence and is highly moistened by the prevailing southwest flow; (b) the air mass exhibits marginal convective instability in the morning and strongly convective instability in the afternoon and evening; (c) both horizontal and vertical shears are weak over the central plateau below 8 km (Fig. 2b). These conditions generally favor development of organized cumulus activity and disturbances driven by latent heat release.

b. The structure of the developing vortices

Presented in Figs. 3 and 4 are vertical cross sections of vorticity, vertical velocity, divergence, relative humidity and temperature for the incipient vortices in case A (12 UTC 13 July) and in case B (12 UTC 27 July), respectively. The geographic locations of the two cross sections are indicated in Fig. 1, respectively, by line segments AA′ for case A and BB′ for case B. The following characteristics regarding the structure of the vortices in their incipient phase are observed.

1) The positive vorticity region is confined near the surface with a vertical thickness of around 3 km. At the level of 8 km, the vorticity approaches zero, and strong negative vorticity dominates aloft; specifically, there is a 180° vertical phase change of the vorticity field between the upper and lower layers (Figs. 3a and 4a). The axes of the maximum vorticity tend to tilt eastward with height. The horizontal radius of the positive vorticity region at the surface is about 300 km in case A and about 400 km in case B. The vertical extent and horizontal dimension of the actual cyclonic circulation are smaller than those illustrated by the positive vorticity region.

2) Ascending motion extends from the surface to the tropopause with its maximum occurring at 8–9 km (about 350–400 mb). However, the center of the maximum vertical velocity does not coincide exactly with the vorticity center. It is located to the east-northeast of the vortex center in case A (Fig. 3b) and to the west-southwest of the vortex center in case B (Fig. 4b).

3) The air converges at the lower layer and diverges at the upper layer. The nondivergence level is between 8 and 9 km, in accordance with the height of maximum vertical velocity (Figs. 3c and 4c).

4) Relative humidity over the surface vortex region

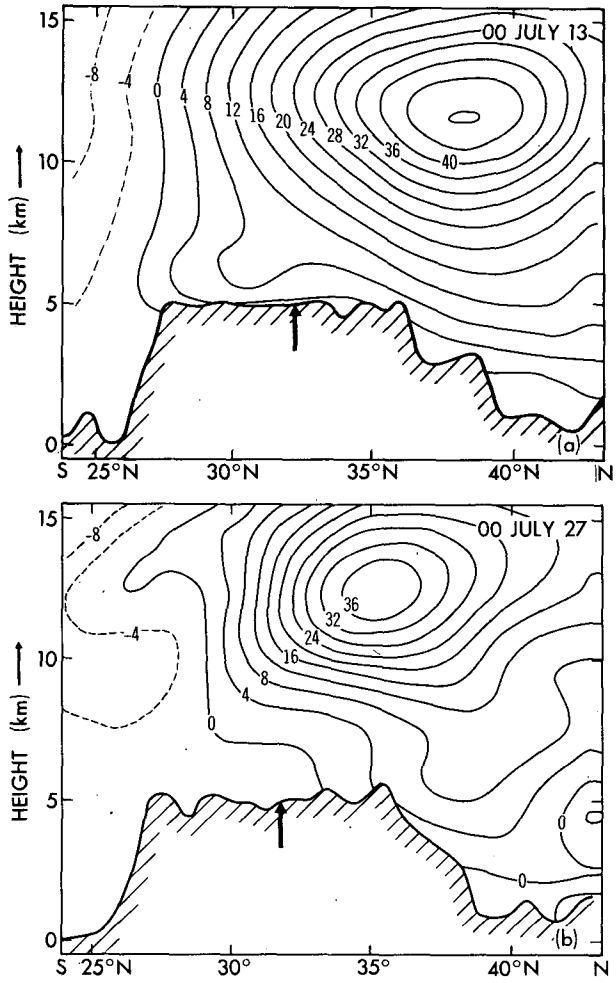

FIG. 2. Plots of vertical cross sections along (a) 92.5°E at 00 UTC 13 July 1979 and (b) 90°E at 00 UTC 27 July 1979, showing zonal velocity contours in units of m s^{-1}. The arrows indicate the locations of corresponding vortex centers formed 12 h later.

is much higher than over its surrounding regions. The moist centers are in good agreement with the locations of the maximum vertical velocity (Figs. 3d and 4d). In case A, a sharp decrease of relative humidity above 10 km is due to the termination of the humidity data at the 300-mb level in ECMWF/FGGE IIIb data. The meridional cross sections across vortex centers (not shown) indicate that the maximum humidity regions lie in the southern part of the vortices with the maximum mixing ratio exceeding 6 g kg^{-1} at 500 mb.

The distribution of the temperature field exhibits somewhat different features between cases A and B. In case A, warmer air spreads over the west part of the vortex from the ground up to 11 km (Fig. 3d), whereas in case B, warmer air covers the west part of the vortex only below 8 km. Above that level the east part of the vortex is warmer (Fig. 4d). This feature is not unlike the structure of the plateau vortices described by Luo

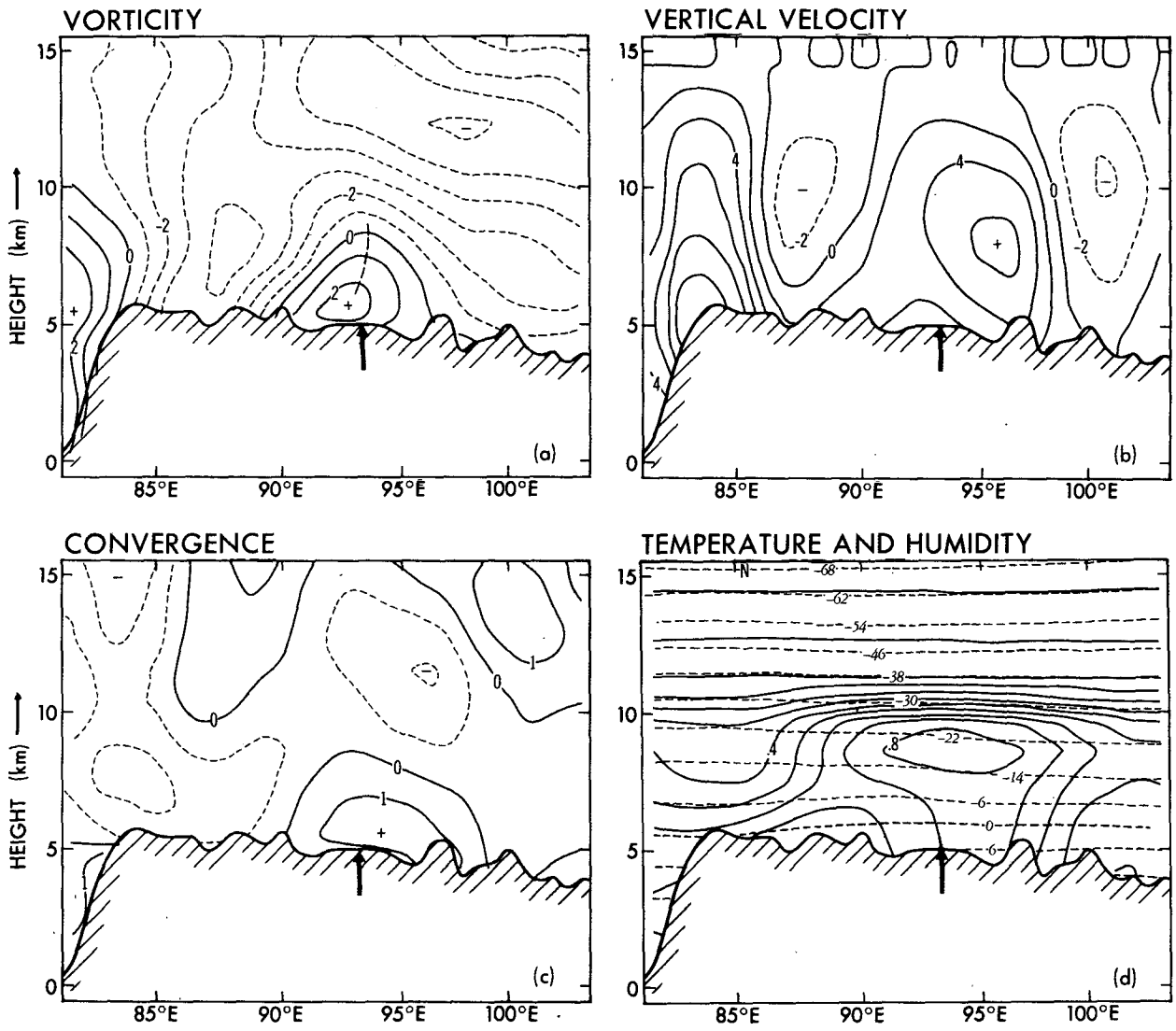

FIG. 3. Plots of cross sections of (a) vorticity (10^{-5} s^{-1}), (b) vertical velocity (cm s^{-1}), (c) horizontal convergence (10^{-5} s^{-1}), (d) relative humidity (solid curve) and temperature (dashed curve in units of °C) along line segment AA′ shown in Fig. 1 at 12 UTC 13 July 1979. The arrows indicate the vortex center in case A.

(1979) and Lu et al. (1984). Their analyses show that a warm center is located to the west of the vortex center at 500 mb. In spite of the differences in detailed structures between cases A and B, the general features for both cases are basically common in their incipient stage.

c. *The circulation conditions favorable for eastward movement*

We now compare the environmental circulation for cases A and B in their maintenance phases (i.e., 12 h later after their formation) in an effort to identify the factors which may be relevant to their movement and maintenance.

A salient difference lies in the environmental mean flow condition. A small-amplitude, quasi-geostrophic disturbance is, to a large extent, steered by the environmental flow. In the presence of vertical shear, it may be relevant to think of a "steering level" for a latent heating-driven vortex that is vertically coupled through convection. The height of this level depends on the vertical heating distribution and the mean wind. When the basic flow increases constantly with height, a heating profile with a lower maximum, and the presence of the boundary layer friction tend to slow down the propagation speed of the unstable disturbances (Wang and Barcilon, 1986). This means that a shallow disturbance that corresponds to a lower maximum heating has a lower steering level; besides, since cu-

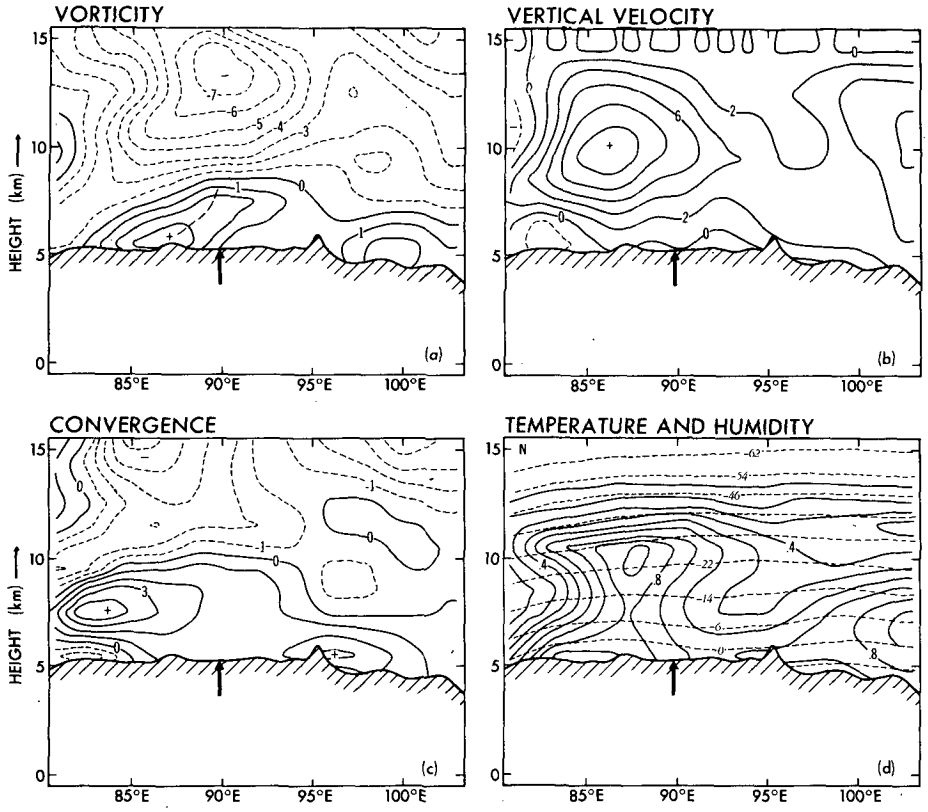

FIG. 4. As in Fig. 3, except that the cross section is along BB' shown in Fig. 1 at 12 UTC 27 July 1979 (case B).

mulus heating is probably mainly sustained by moisture convergence in the planetary boundary layer, migration of the disturbance appears to closely relate to the mean wind at lower layers. For instance, in his study of tropical Atlantic disturbances, Shapiro (1986) found that the advection by the mean wind is much more important to vorticity phase propagation at lower levels (e.g., 850 mb) than upper ones. For the plateau vortices, 7–8 km (i.e., 2–3 km above the terrain) may be a reasonable height for the steering level. This level is also close to their nondivergence level. If one assumes 7.5 km to be the steering level, then the steering speed is around 12 m s^{-1} in case A, while only about 5 m s^{-1} in case B. If one takes a vertically averaged zonal wind from the surface to 200 mb as an indicator, the average mean velocity would be 14 m s^{-1} in case A but merely 5 m s^{-1} in case B. The vortex that later moved out of the plateau (case A) had a much stronger steering speed in its environment. The observed mean eastward-propagating speed of the plateau vortices is 5–6 deg of latitude per day (Qian, et al., 1984a). Over the central plateau (e.g., Naqu), the prevailing wind in July at 7–8 km is westerly (wind direction between 225° and 315°) with a zonal component of 7 m s^{-1}, which is close to the climatological value of the phase speed of the plateau vortices.

Some other differences in the background circulation and structures are also noticed but with less certainty. The mature vortex in case A was located at the southeast of an eastward-migrating westerly trough, whereas the mature vortex in case B was located near the eastern end of a weak surface shear line, and another low vortex had just formed at the western end of the shear line (Fig. 5). Between the two vortices an anticyclonic circulation separated the mature vortex from the westerly flow. It appears that the separation of the surface vortex from the waves in the westerlies prohibits its eastward movement and intrusion of cold air. The differences in their structure between cases A and B are a) the northerly flow behind the vortex center is stronger than the southerly flow ahead of the center in case A, while the opposite is true for case B; (b) the vortex in case A has lost its warm structure, but the vortex in case B still maintains its warm structure.

The maintenance and eastward movement seem to depend upon the environmental mean flow conditions; this is particularly true in the vorticity advection and weak cold air intrusion associated with the translating waves in the westerly flow north of the plateau. In the absence of the favorable circulation condition, the vortices can not maintain themselves, especially as they move downslope toward the lee side of the plateau.

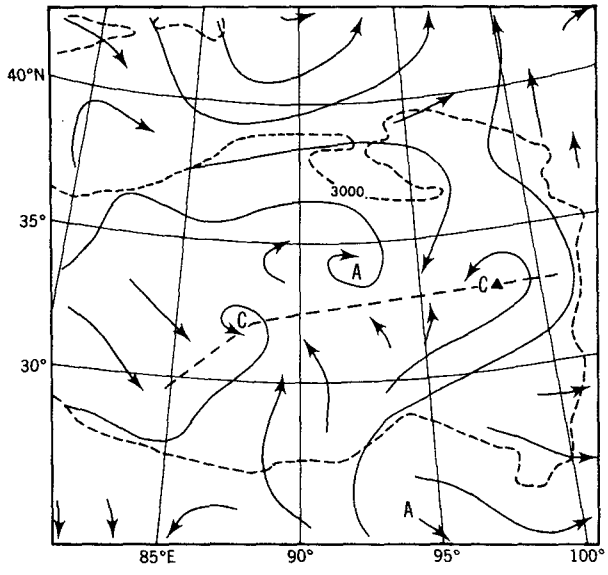

FIG. 5. Streamline analysis at 5500 m for 00 UTC 28 July 1979 (case B). The triangle indicates the location of the mature vortex. The thick dashed curve shows the surface convergence line. The thin dashed curve is 3000 m height contour.

This suggests that their development and maintenance are crucially influenced by the thermal and dynamic effects of the elevated plateau terrain. Further theoretical analysis and discussion will be presented in section 4.

3. Numerical experiments

As has been discussed in section 2, both horizontal and vertical shears below 8 km over the plateau are weak prior to the genesis of the plateau vortices suggesting that the local available potential energy and kinetic energy of the mean flow are not likely to be major energy sources. On the other hand, it has been recognized for a long time that the release of latent heat of condensation represents an important source of energy for midlatitude precipitating synoptic-scale disturbances (Aubert, 1957; Danard, 1964, Tracton, 1973; Smith et al., 1984). The development of the plateau vortices are frequently accompanied by an appreciable amount of convective precipitation, pointing to the importance of the latent heating in the generation of eddy available potential energy.

To assess the role of latent heating and dynamic instability in the development of the Tibetan Plateau vortices in the rainy season, numerical experiments are performed with real data using a regional primitive equation model. The principle difficulties in the simulation of the plateau vortices are twofold. The first is caused by the scarcity of the observations for the initial condition on the regional scale, especially over the western plateau. The second is associated with the increasing importance of modeling diabatic, topographic and surface effects. The severe limitation in the density of the initial data makes it extremely difficult to study the genesis of the vortex in the western plateau (west of 90°E). The vortex to be simulated here generated and developed east of 90°E, where rawinsonde data are relatively dense. We choose this case from July 1979, because an enhanced database supplemented by MONEX and coherent global analysis were available during this period.

The model employed here is a modified version of the GFDL mesoscale model (Ross and Orlanski, 1982), which includes the dynamic effect of a model topography (Orlanski and Polinsky, 1984). It uses a Cartesian coordinate system with the height z as vertical coordinate. The horizontal grid resolution is 60 km and the vertical grid spacing is 1 km with the model lid located at approximately 15 km. An explicit formulation of moist convection was used, with a latent heating term included in the thermodynamic equation. Condensation is assumed to occur when the mixing ratio exceeds an effective saturation mixing ratio, kqs. The factor k should depend on the grid resolution, Δx, and environmental conditions under which the condensation takes place (Smagorinsky, 1960; Miyakoda et al., 1969). A value for k of 0.85 was taken here in view of the present grid size Δx of 60 km and the fact that observed relative humidity in clouds over the plateau is generally smaller than that over eastern China (Qian et al., 1984b). The model includes a prognostic equation for condensed water. When cloud water content exceeds a threshold value, C_r, the excessive cloud water is assumed to precipitate immediately and is removed from the air column without consideration of evaporation of rain drops in the lower, unsaturated layers. The value for the threshold of cloud water loading, C_r, used here is 1.5 g m^{-3}. The cloud fraction function, which specifies fractional cloud coverage in a grid column of horizontal area Δx^2, is assumed to be a constant value of 0.85. The ground temperature is specified using FGGE data.

The present model includes the high-resolution terrain shown in Fig. 1. To simulate the influence of the topography, a large viscous stress term is incorporated into the model's momentum equation. At the terrain surface, the mountain body drag reduces to a specified surface drag. A surface drag coefficient of 1.25×10^{-3} was used in the model. For an underground layer, the mountain drag coefficient is assumed to be 240 times as large as the surface drag coefficient. Since this procedure effectively diminishes the wind velocity inside the mountain configuration to very small values, the blocking and the surface drag effects of a high and steep topography can be simulated reasonably well (Wang and Orlanski, 1987). At the surface of the viscous mountain, there exist heat and moisture fluxes which are proportional to the corresponding temperature and moisture gradients, respectively. These surface fluxes are produced mainly by eddy vertical dif-

fusivity with a small portion by the vanishingly small vertical motion that does not exactly vanish at the surface. Although large viscosity within the mountain configuration dramatically suppresses the motion within the mountain, since the vertical velocity at the terrain surface was not forced to be zero exactly, the surface heat and moisture fluxes may be slightly affected by the vertical motion outside the mountain. This is apparently a weakness of the present topographic parameterization. Nevertheless, the purpose here is not to assess the influence of the surface fluxes on the development but rather to determine the effect of latent heat release. The initial distribution of the temperature below the terrain surface (down to 2 km depth) was assumed to form a constant lapse rate of 6.8°C km^{-1} for the simulations both with and without latent heating. This lapse rate is close to the monthly mean lapse rate for the troposphere over the plateau.

The data used for initial and boundary conditions in the numerical simulations were taken from the ECMWF/FGGE IIIb analysis for case A. To focus on the initial development, a 36-h simulation started from 00 UTC 13 July 1979 was performed, with emphasis on the analysis of the first 24-h solution.

Figure 6 compares 500-mb vorticity fields at 12 UTC 13 July (hour 12) and 00 UTC 14 July (hour 24) for the ECMWF/FGGE analysis (panels a and b), the control simulation with latent heating (panels c and d), and the simulation without latent heating (panels e and f). Figure 6c shows that a positive vorticity center forms in the control simulation at hour 12 (near 32.5°N, 92°E) that is close to the vorticity center from the FGGE analysis and the subjectively analyzed vortex center (Table 1). At hour 24, this vortex further intensified and moved to the eastern plateau (around 34°N, 98.5°E); at the same time, another positive vorticity region seems to be generated in the central plateau (near 35°N, 91°E) (Fig. 6d). Notice that the corresponding FGGE analysis at 00 UTC 14 July only shows a broad region of positive vorticity elongated in the east–west direction and between 90° and 100°E; it fails to identify two separate vorticity centers due to its crude resolution of 187 km. However, the weather map published by the State Meteorological Administration of the PRC and the subjective analyses by Qian et al. (1984a) and by Qin and Cui (1984) all indicate two separate vortices at 00 UTC 14 July (Table 1). The control simulation of the locations of vortex-genesis by the mesoscale model agrees better with the subjective analysis than the FGGE analysis; the former has higher resolution and exhibits more details than the latter.

Figures 7a and 7b illustrate vertical profiles of vorticity and temperature along the meridional line segment CC′ indicated in Fig. 1 at 00 UTC 14 July. Notwithstanding minor discrepancies, the overall similarity in the vortex structure between the FGGE analysis and the control simulation are summarized as follows. The cyclonic vorticity region is isolated over the middle of the plateau terrain and confined to the lower layer below 8–9 km; there is a 180° phase shift in the vorticity field between the upper and lower levels; warm air covers the central and southern part of the vortex. The latitude of the simulated vorticity center at hour 24 is about 1° latitude north of the observed one. Correspondingly, the region of 24-h accumulated precipitation is located 1°–2° latitude north of the observed rainfall region, but the amount of total rainfall and the size and shape of the precipitating area are comparable (Fig. 8). The most noticeable difference between Fig. 7a and 7b is that the simulated positive vorticity region of the vortex exhibits smaller horizontal dimension and has a significantly stronger intensity compared with the FGGE analysis. This difference can be partially accounted for by the incompatible grid size: the FGGE analysis uses a grid resolution of 187 km, which is three times as large as the present model resolution. If the model results are averaged over an area of $9\Delta x^2$, where Δx is the horizontal resolution, the maximum vorticity of the vortex will be reduced and its horizontal dimension will increase. Overall, the control simulation provides a reasonable solution.

On the other hand, without latent heating, the simulation produces no evident development of cyclonic vorticity at 500-mb after 12 h at the east-central plateau (region between 90° and 95°E) (Fig. 6e). After 24 h, the vorticity centers that occurred in the control simulation are still absent in the simulation without latent heating (Fig. 6f). Comparing the meridional cross section of vorticity for the nonheating simulation (Fig. 7c) with that for the control simulation (Fig. 7b), we see clearly that the discrepancy is evident only in the vicinity of the vortex in the control simulation located around 34°N, where precipitation and release of latent heat took place.

The sharp contrast between the simulations with and without latent heating demonstrates that, without latent heat release, the dynamic instability of the environmental flow over the plateau is unable to generate the low-level vortex, but the latent heat released from 5–10 mm precipitation can produce a vortex with a strength comparable to observations in the case studied here.

4. The development mechanism

a. The hypothesis

The numerical experiments for the selected case suggest that the latent heating is an essential energy source for the growth of the plateau vortices in the rainy season. We now further confirm and elaborate this notion by showing climatological characteristics of the plateau environment.

As noticed by Yeh (1979), the environmental conditions for the formation of the plateau vortices are in many respects similar to those for the growth of tropical cyclones, even though the plateau vortices have much

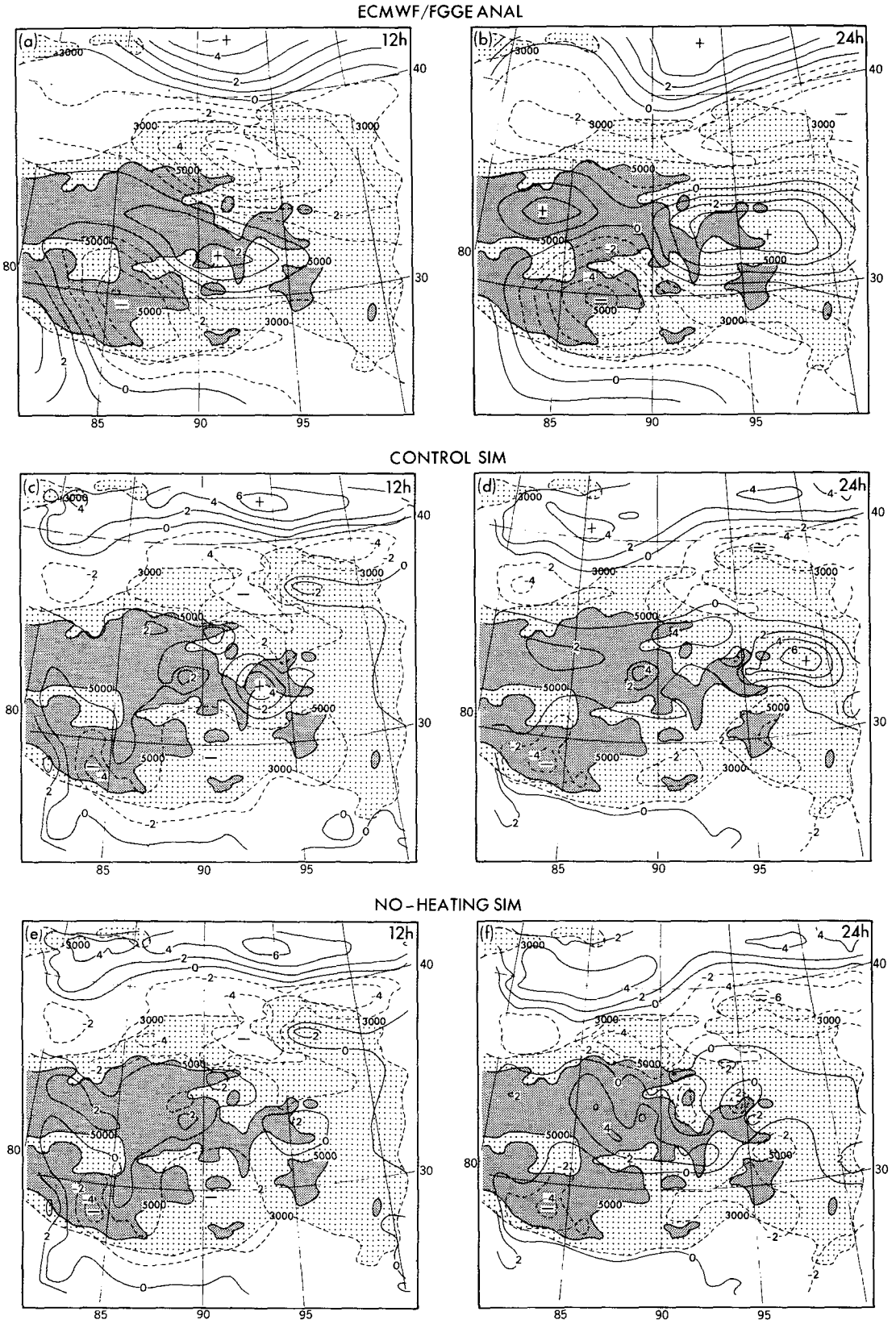

FIG. 6. Plots of 500-mb vorticity at 12 and 24 h from (a) and (b) respectively, ECMWF/FGGE IIIb analyses for 13–14 July event; (c) and (d), respectively, control simulations, (e) and (f), respectively, the simulation without latent heating. Units are in 10^{-5} s^{-1} for FGGE analysis and are 2×10^{-5} s^{-1} for the simulations. The light and dark shading areas indicate the regions where topographic heights are 3000–5000 m and over 5000 m, respectively.

TABLE 1. Comparison of the geographic locations of the vortices in case A for different analyses.

Analysis type	Date		
	12 UTC 13 July	00 UTC 14 July	12 UTC 14 July
A. Weather map	33°N, 92.5°E	34°N, 98°E 33°N, 90°E	35°N, 104°E
B. Qin and Cui (1984)	33°N, 92.5°E	34.5°N, 97.5°E 34°N, 91.3°E	35.3°N, 105.2°E
C. Qian et al. (1984a)	34°N, 94°E	34°N, 98.5°E 34°N, 91.5°E	34.5°N, 101°E
D. ECMWF/FGGE analysis (*vorticity center*)	32°N, 91.5°E	(32.5°N, 96°E)	34°N, 101.5°E

weaker intensity and a much shorter life span (about 1 day) due to absence of durable moisture supply and the occurrence of a remarkable diurnal variation. During the summer, the Tibetan Plateau is a vast heat source to the troposphere. As a consequence, on the monthly mean chart for July, the upper tropospheric flow is characterized by an anticyclonic circulation over the plateau (the Tibetan high) with the westerly jet stream and the polar front to the north and the subtropical easterly jet to the south. The plateau boundary layer is occupied by a large low pressure system which is elongated in the east–west direction and contains

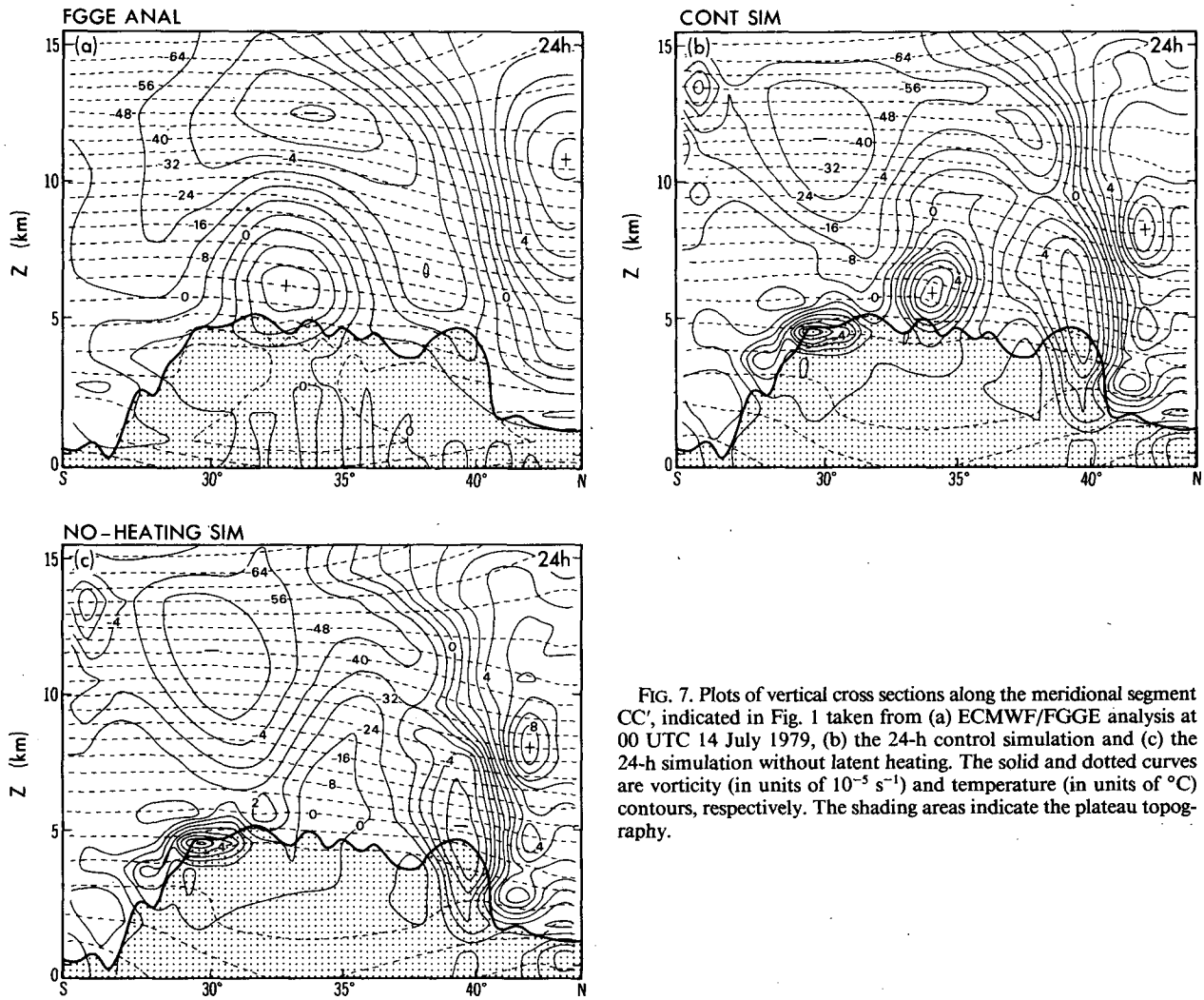

FIG. 7. Plots of vertical cross sections along the meridional segment CC′, indicated in Fig. 1 taken from (a) ECMWF/FGGE analysis at 00 UTC 14 July 1979, (b) the 24-h control simulation and (c) the 24-h simulation without latent heating. The solid and dotted curves are vorticity (in units of 10^{-5} s^{-1}) and temperature (in units of °C) contours, respectively. The shading areas indicate the plateau topography.

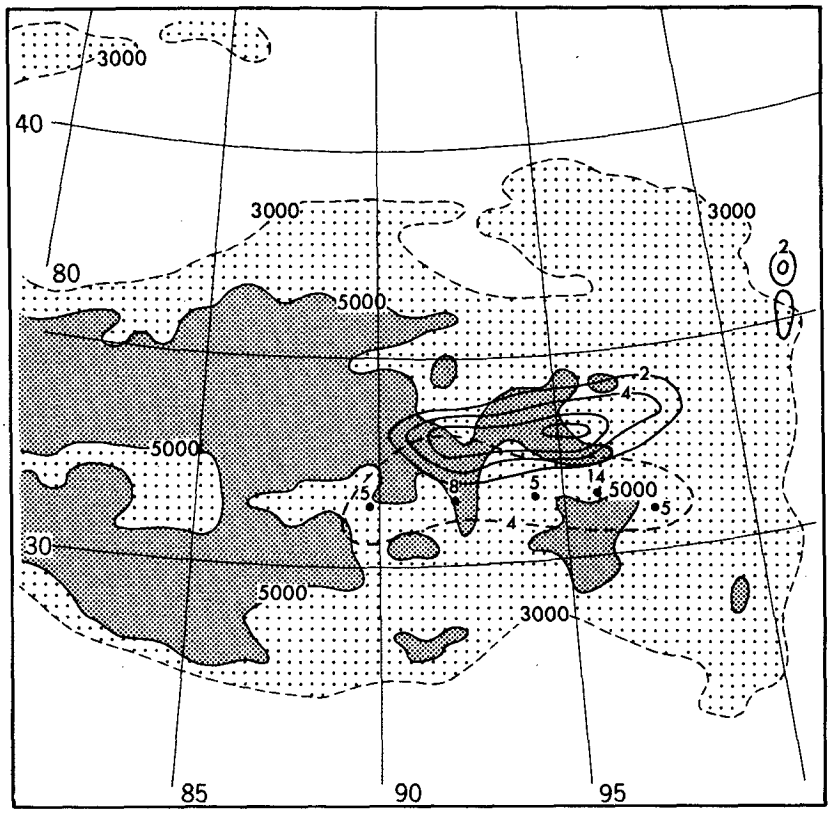

FIG. 8. Distributions of accumulated 24-h precipitation, in units of mm, starting from 00 UTC 13 July, as taken from observation (dashed curves) and the control simulation (solid curves). The shading has the same meaning as in Fig. 6.

several mesoscale lows that are located along an east–west-oriented surface shear line (Yeh, 1981). The convergence zone associated with the surface shear line is a productive source region for the plateau warm vortices. The flow is southerly to the south of the surface shear line, and is often connected with the Indian monsoon and transports water vapor from northern India and the Bay of Bengal into the plateau region through the valleys of the Himalayas. Due to this moisture transport and the evaporation from the plateau surface, a climatological moist center in middle troposphere stands out in the southeastern part of the plateau (Shen, 1979). The presence of this moist boundary layer favors conditional instability and the development of convective precipitation.

The similarities are evident between the atmospheric thermal structure over the summer plateau and the one over a tropical ocean. Figure 9 illustrates a mean sounding (bold solid curve) in July 1981 at 12 UTC from Lhasa (29°40′N, 91°08′E). This mean sounding is, to a great extent, representative of conditions in the air over the central plateau where, climatologically, plateau vortices most frequently occur. We note that the atmosphere is in a conditionally unstable state, the lifting condensation level is around 540 mb, and a deep layer of positive bouyancy extends from 500 to 170 mb. It is believed that the low-level convergence, which is induced by surface shear lines, mesovortices and numerous mountain peaks acting as "heat islands" and enhanced by surface friction, is directly responsible for the initiation of the cumulus convection. Observations have shown that during the rainy season of 1979, convective clouds constituted over 90% of the total amount of cloudiness, and the mean cloud coverage in the afternoon and evening was in excess of 80% in the central plateau region (Qian et al., 1984b). The plateau in summer is a region of high convective activity: there are many more thunderstorms, hailstorms, showers and convective clouds here than anywhere else in the same latitude belt (Gao, et al., 1981). These observations appear to support the hypothesis that the organized release of cumulus latent heat could be a major driving force for the growth of the plateau vortices.

Using a linear, quasi-balanced multilayer model, Charney and Eliassen (1964) demonstrated that instability could result from the cooperative interaction between cumulus convection and large-scale motion, which was referred to as CISK. Because of the limitations of the model assumptions, such as balanced motion, and the neglect of nonlinearity and surface energy

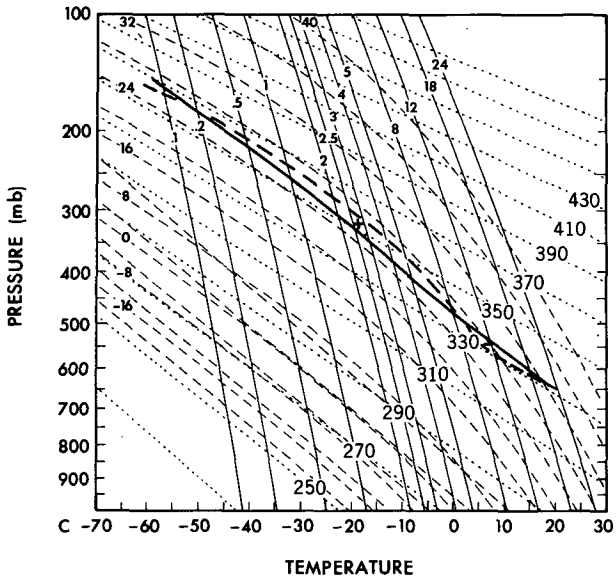

FIG. 9. The monthly mean sounding (thick solid curve) at 12 UTC for July 1981 at Lhasa (29°40'N, 91°8'E).

fluxes, tropical CISK has fundamental difficulties in explaining the growth of tropical storms (Emanuel, 1986). As a matter of fact, in view of the basic assumptions of the model, the theory is more relevant and useful in interpreting the growth of those systems driven by convective latent heating that are smaller in amplitude and shorter in duration but strongly affected by the earth's rotation. In the presence of sufficiently strong planetary vorticity, and a weak preexisting, large-scale convergence, the organized release of latent heat in large numbers of cumulus towers and cumulonimbi may generate an amplifying synoptic- or subsynoptic-scale rotational system, if the moisture supply sustaining convection mainly comes from the large-scale convergence in the subcloud boundary layer and if the moisture content of the boundary layer exceeds a minimum threshold value (Wang, 1987a). There is no reason to restrain a small-amplitude instability resulting from the interaction between cumulus and synoptic motions to maritime events. In what follows, the previously mentioned hypothesis will be tested by examining whether CISK can develop in the plateau environment, and by revealing the mechanisms responsible for the development if CISK is possible.

b. *Theoretical model and choice of parameters for the plateau environment*

The theoretical model used here is similar to that described in detail by Wang (1987a). For large-scale flow, the lowest-order nondimensional vorticity and thermodynamic equations for small perturbations about a uniform zonal flow with speed U may be written as

$$\left(\frac{\partial}{\partial t}+U\frac{\partial}{\partial x}\right)\nabla^2\phi=\frac{\partial\omega}{\partial p}, \tag{4.1a}$$

$$\left(\frac{\partial}{\partial t}+U\frac{\partial}{\partial x}\right)\frac{\partial\phi}{\partial p}+S(p)\omega=\epsilon\frac{\eta(p)}{p}\omega_m, \tag{4.1b}$$

with the upper and lower boundary conditions

$$\omega=0 \quad \text{at} \quad p=p_u, \tag{4.2a}$$

$$\omega=-r\nabla^2\phi \quad \text{at} \quad p=p_e, \tag{4.2b}$$

where U, ϕ and ω represent, respectively, the nondimensional mean zonal velocity, geopotential height and vertical p-velocity; the other nondimensional numbers or functions are

the nondimensional static stability parameter,

$$S=\sigma^*P_0^2/f_0^2L^2, \tag{4.3a}$$

the coefficient of latent heating intensity,

$$\epsilon=\tilde{\alpha}\bar{q}\frac{RL_c}{f_0^2L^2C_p}, \tag{4.3b}$$

and

the coefficient of Ekman layer dissipation,

$$r=\frac{\rho_e gL}{P_0V}\left(\frac{A_zf_0}{2}\right)^{1/2}. \tag{4.3c}$$

In (4.3), σ^* denotes the static stability parameter of the basic state, defined by $\sigma^*=-RP_0^{-1}(\partial T/\partial p-RT/C_pP_0)$, where T is the basic state temperature; the quantities L, V and P_0 are basic horizontal length, horizontal velocity and pressure scales, respectively; constants R, C_p and L_c are, respectively, the gas constant, the specific heat of the air at constant pressure and the latent heat of condensation. Quantity $\tilde{\alpha}$ is a heating intensity factor measuring the ratio of convective precipitation to the total amount of moisture that converges into the cumulus cloud ensemble; in reality, $\tilde{\alpha}$ should be less than unity. The physical meanings of the quantities ρ_e, A_z, $\bar{q}$, f_0, p_u and p_e are explained in Table 2. The vertical p-velocity, ω, is assumed to vanish at the upper boundary p_u and to be proportional to the relative vorticity, (by matching the vertical velocity induced by Ekman pumping) at the top of the boundary layer, p_e, which also serves as the model's lower boundary. The instability crucially depends upon the vertical heating distribution, $\eta(p)$, and the nondimensional static stability parameter, $S(p)$, that is a function of the stratification and the Coriolis parameter.

The central latitude of the f-plane is assumed to be at 31°N, corresponding to $f_0=0.75\times10^{-4}$ s^{-1}. For the turbulent viscosity coefficient, A_z, the value of 20 m^2 s^{-1} has been used in view of the surface roughness and the unstable condition in the boundary layer due to strong sensible heating. The upper boundary is located at 100 mb, which is close to climatological tropopause level (96 mb in July), and the plateau surface

is at 600 mb (about 4300 m). The pressure at the top of the boundary layer is chosen to be $p_e^* = 530$ mb (about 5400 m). The air density at p_e^* is assumed to be 0.67 kg m^{-3}.

The moisture content in the plateau boundary layer during the summer monsoon season is considerably higher than that in the surrounding region. For instance, the monthly mean specific humidity at 12 UTC over the central plateau averaged for stations Lhasa and Naqu in July 1981 is 5.2 g kg^{-1} at 500 mb and 8.4 g kg^{-1} at 600 mb, while the corresponding values east of the plateau at Wuhan (30°30′N, 114°04′E) are only 3.2 g kg^{-1} at 500 mb and 5.6 g kg^{-1} at 600 mb. Based upon the monthly mean profile at 1200 UTC for the central plateau region, the mean specific humidity in the model boundary layer from 600 mb to 530 mb should be 7.2 g kg^{-1}. For vigorous convective days, this value may exceed 7.5 g kg^{-1} as deduced from the analysis of Qian et al. (1984b). A value of 7.0 g kg^{-1} is utilized in the present computation.

The heating function $\eta(p)$ in (4.1b) is specified by the following cubic function of nondimensional pressure with two adjustable shape parameters a and p_1:

$$\eta(p) = \begin{cases} 0, & p < Pt \quad \text{or} \quad p > Pb, \\ A[a(p_1-p)(p-Pt)^2 \\ \qquad +(1-a)(p_1-p)^2(p-p_t)], & p_t \le p \le p_b, \end{cases} \tag{4.4}$$

where p_b and p_t represent the cloud base and top, respectively; the coefficient A which satisfies the constraint $\int_0^1 \eta(p)dp = 1$ is

$$A = \left\{ \frac{1-2a}{4}(p_b^4 - p_t^4) + \frac{1}{3}[3a(p_1+p_t) - 2p_1 - p_t] \times (p_b^3 - p_t^3) + \frac{1}{2}[p_1(p_1+2p_t) - a(p_1^2 + p_t^2 + 4p_1p_t)] \times (p_b^2 - p_t^2) + p_1p_t[a(p_1+p_t) - p_1](p_b - p_t) \right\}^{-1}. \tag{4.5}$$

The profile (4.4) can approximate various types of heating distributions by adjusting the parameters a and p_1 (Wang, 1987a).

The height of the convective cloud base over the plateau is higher than over the plain region. For instance, analysis of observed balloon data shows that the average height of the cloud base for cumulonimbi is about 1500 m over the central plateau but only several hundred meters over the Sichun Basin and the Yangzi River Valley. The lifting condensation level derived from the profiles of temperature and dewpoint for the period of vigorous convection over the central-eastern plateau is generally below 500 mb (Qian et al., 1984b). Based upon the mean sounding shown in Fig. 9, a cloud base, p_b^*, of 530 mb is assumed, which is a little above the lifting condensation level. The cloud top, p_t^*, is set at 200 mb (about 12.5 km), which is slightly lower than the upper boundary of the positive bouyancy layer for the undiluted ascent of moist air shown in Fig. 9. This is also in good agreement with the observed average height of the top of cumulonimbi during the rainy season over the central plateau, which is 8 km above the surface (Qin et al., 1984). The shape parameters, a and p_1, in the heating parameterization are difficult to estimate because observations are not available. The values $a = 1$ and $p_1 = p_b$, however, are tentatively set. This heating profile, which is based on the monthly mean sounding data and radar observations, is referred to as model heating profile 1 and is shown by the solid curve in Fig. 10. To avoid the uncertainty in choosing a and p_1, another model heating profile (referred to as model heating profile 2) is proposed in full accordance with the results of the numerical simulation. The profile 2 is characterized by the parameters, $p_t^* = 250$ mb, $p_b^* = 530$ mb, $a = 0.0$ and $p_1^* = 620$ mb, and shown by the dash-dotted curve in Fig. 10. Table 3 compares the normalized model heating profile 2 with the normalized profile that is deduced from the amount of simulated cloud water content at the vortex center at 00 UTC July 14. It is seen that the model heating profile 2 is in good agree-

TABLE 2. List of the model parameters used for the Tibetan Plateau and tropical environments. The quantities p_m, p_e, p_b, p_u, p_t and p_1 are nondimensionalized by the pressure scale $P_0 = 1000$ mb.

Model parameters	Tropical environment	Tibetan Plateau environment
f_0, Coriolis parameter (s^{-1})	0.377×10^{-4}	0.75×10^{-4}
A_z, eddy viscosity coefficient (m^2 s^{-2})	10	20
σ_0^*, model static stability parameter at 1000 mb (m^2 s^{-2} mb^{-2}) in (4.5)	0.01	0.006
$\bar{q}$, mean specific humidity in moist layer (g kg^{-1})	18.0	7.0
p_m, pressure at the top of the moist layer	0.90	0.53
p_e, pressure at the top of the Ekman layer	0.90	0.53
p_b, pressure at the cloud base	0.90	0.53
p_t, pressure at the cloub top	0.10	0.20
p_u, pressure at the upper boundary	0.10	0.10
p_e, density at p_e (kg m^{-3})	1.20	0.67
α, heating factor	1.0	1.0
p_1, shape parameter	0.90	0.53
a, shape parameter	1.0	1.0
$\alpha\bar{q}_c$, minimum threshold mean specific humidity in the moist layer (g kg^{-1})	14.0	5.5
$\bar{q}/\alpha\bar{q}_c$, the CISK index	1.30	1.30

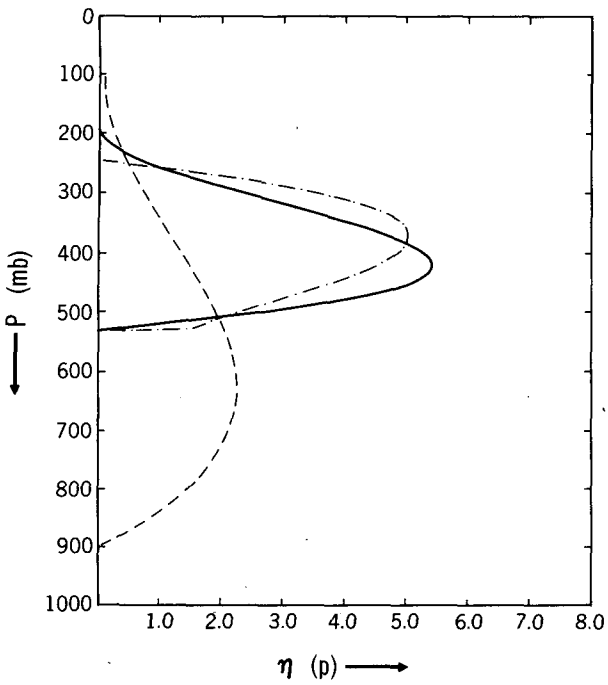

FIG. 10. Heating profiles for a tropical environment (dashed curve) and for an environment over the summer Tibetan Plateau: model heating profile 1 (solid curve) and model heating profile 2 (dash-dotted curve).

ment with the vertical heating distribution in the numerical simulation at the incipient phase of the vortex. Both model heating profiles will be used in estimating the rate of growth.

The basic state stratification that is defined by σ^* is assumed to be a function of pressure only and is computed from the observed monthly mean temperature profile, $T(p)$, over the central plateau and at 12 UTC in July by means of spline fitting. (This profile is hereafter referred to as the observed stratification.) The solid and dotted curves in Fig. 11 show the observed vertical profiles of the static stability parameter in July 1981 at 12 UTC for the central plateau and for Wuhan, respectively. The midtropospheric static stability over the plateau is substantially smaller than that at the same level off the plateau (at Wuhan) due to the strong sensible heat flux from the elevated surface: the mean static stability at 500 mb is 2.4×10^{-2} m^2 s^{-2} mb^{-2} at the central plateau versus 4.0×10^{-2} m^2 s^{-2} mb^{-2} at Wuhan. The monthly average lapse rate between the surface and 200 mb is 7.2 C km^{-1} for the plateau and 6.2 C km^{-1} for Wuhan.

c. *Discussion of the model results*

Computations have been carried out of the growth rate and the vertical structure of the CISK disturbance in an environment similar to that over the plateau. A shooting method (Langer, 1960) was employed to numerically solve the eigenvalue problem for the instability. The numerical calculations were checked by using the analytical solution given by (3.6) of Wang (1987a) for an ideal model stratification,

$$\sigma^*(p) = \sigma_0^*/p^2, \tag{4.6}$$

which is a fairly good approximation for the observed one.

Figure 12 displays the growth rates as functions of nondimensional wavenumber k for several sets of parameters. The solid curve shows the growth rate for parameters typical of the Tibetan Plateau environment in July (given in Table 2). It is computed using the model heating profile 1 and the observed stratification profile shown by the solid curve in Fig. 11. It is seen that the growth rate reaches a maximum value of about 0.46 day^{-1} at a wavelength around 800 km or a dimension of the depression of about 400 km. The growth rate shown by the dash-dotted curve in Fig. 12 is computed for the same parameters for the plateau but using the model heating profile 2. Both heating profiles lead to qualitatively similar behavior for the instability, although the heating profile 2 tends to favor the amplification of shorter waves.

The vertical structure of the corresponding most unstable CISK mode (wavelength is 800 km) is presented in Fig. 13. It is characterized by a low geopotential height below 400 mb with a minimum occurring around 500 mb and by a high geopotential height above 400 mb with a maximum around 300 mb. A 180° phase change in vorticity and geopotential height fields is seen between the upper and lower layers. The positive vorticity region is confined to a shallow layer near the surface. Upward motion exists over the entire vertical model domain with a maximum around 440 mb. This level corresponds also to a nondivergence level. A warm core structure can be found between 500 mb and 350

TABLE 3. Comparison between the normalized model heating profile 2 and the normalized heating profile that is constructed from the results of the numerical simulation.

	Pressure (mb)							
Model	250	300	350	370	400	450	500	530
Numerical model heating profile	0.00	0.42	0.96	1.00	0.92	0.71	0.50	0.33
Model heating profile 2	0.00	0.68	0.97	1.00	0.96	0.77	0.48	0.30

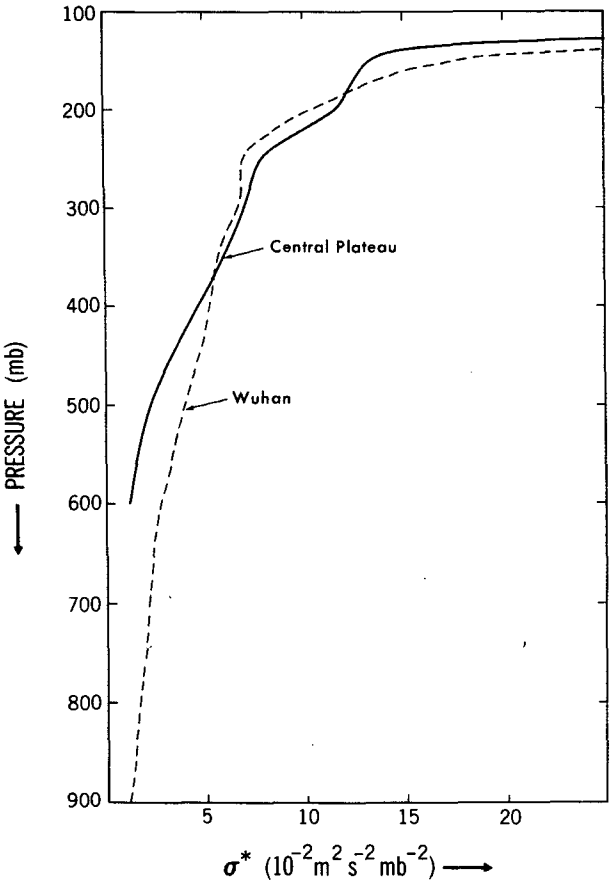

FIG. 11. Profiles of the static stability parameters (in units of 10^{-2} $m^2 s^{-2} mb^{-2}$) calculated from the observed monthly mean temperature in July 1981 at 12 UTC from the central plateau (solid curve) and from Wuhan (30°38'N, 114°04'E), (dashed curve).

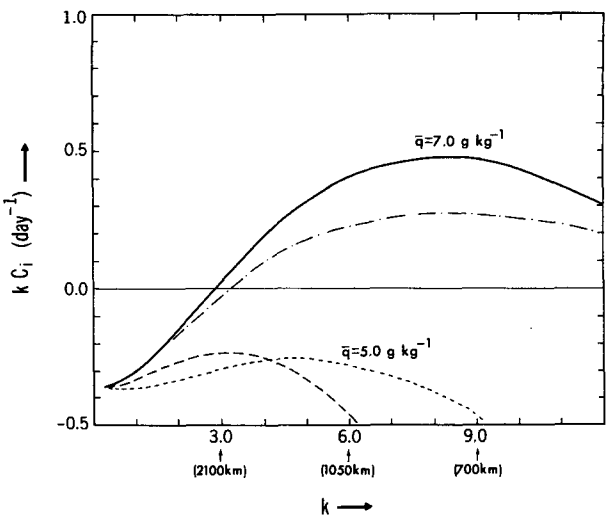

FIG. 12. Plots of CISK growth rate as a function of the wavenumber k for different parameters settings. All of the parameters not explained in the text are listed in Table 2 for the plateau environment. The solid and dashed-dotted curves are calculated using model heating profile 1 and 2, respectively. The dashed curve is obtained by changing only the stratification profile over central plateau to that over Wuhan. The dotted curve is obtained by changing only the boundary layer specific humidity from 7 to 5 g kg^{-1}.

mb. In general, the structure of the model CISK disturbance resembles that of observed plateau vortices described in section 2, in spite the model's neglect of variations of the basic zonal flow in both the vertical and meridional directions. Because these variations are hardly significant below 8 km, as was pointed out in section 2, they seem to play only a secondary and indirect role in the dynamics.

Now we examine why a CISK disturbance can grow in the plateau environment, or, to put this in another way, what mechanisms are responsible for the development of the model-predicted mesoscale CISK disturbance. For this purpose, it is very illustrative to compare the *minimum threshold moisture content* that is required for CISK development in the plateau environment with that in a tropical oceanic environment; this minimum threshold moisture content is independent of the Coriolis parameter, the Ekman layer dissipation and wavelength and is basically determined only by the environmental stratification and vertical heating distribution (Wang, 1987b).

We first focus on the effect of differing vertical extent of heating on the CISK development by assuming that, for both environments: 1) the static stability parameter is the same as described by (4.6) with $\sigma_0^* = 10^{-2}$ m^2

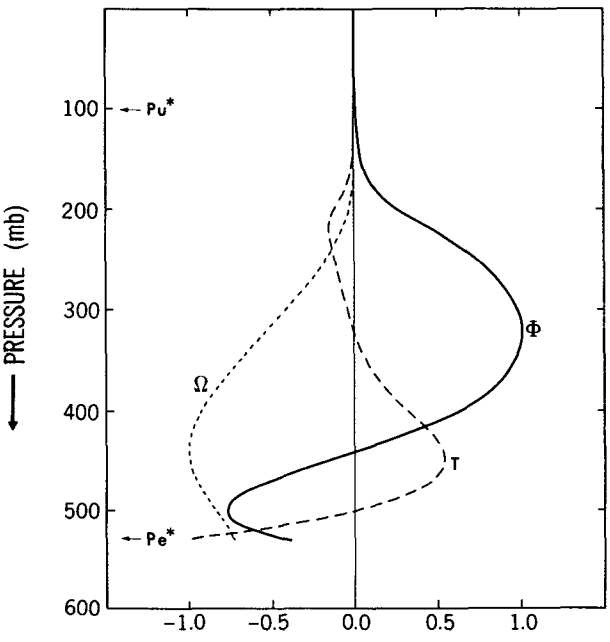

FIG. 13. Plots of the vertical structure of vertical velocity (Ω), geopotential (Φ) and temperature (T) as computed for the fastest growing disturbance in an environment similar to that over the summer Tibetan Plateau.

s^{-2} mb^{-2} and 2) the heating intensity factor, $\tilde{\alpha}$, is the same and the heating profiles are similar, i.e., $p_1 = p_b = p_e = p_m$ and the shape parameter, $a = 1$. The only differences between the two heating profiles are the heights of the cloud top, p_t, and the cloud base, p_b (Table 2 or Fig. 10). With these assumptions, one can calculate, using the Eq. (4.3) of Wang (1987a), the minimum threshold specific humidity, $\tilde{\alpha}\bar{q}_c$, for CISK, which is about 14 g kg^{-1} at a wavelength of 3900 km over a tropical ocean but only 9.2 g kg^{-1} at a wavelength of 1370 km over the Tibetan Plateau. It is clear that the significant reduction in $\tilde{\alpha}\bar{q}_c$ for the plateau environment results from the small vertical extent of the heating, $p_b - p_t$. The development of a CISK disturbance over the plateau requires much less moisture content in the boundary layer, because the latent heat is released in a relatively shallow layer, bounded below by p_b and above by p_t, within which the heat capacity of the air mass in a vertical column with unit area is considerably less than that over a tropical environment.

We observe that the reduced static stability due to the enormous surface sensible heat flux over the plateau further destabilizes the plateau environment. If we now replace σ_0^* by 0.6×10^{-2} m^2 s^{-2} mb^{-2} so as to match the model stratification, (4.6), with the *observed* plateau stratification—σ_0^* was chosen in such a way that σ^* at the level of 500 mb, where the vortex often acquires its maximum strength, is exactly equal to the observed value—the minimum threshold specific humidity over the plateau then decreases considerably to a value of 5.5 g kg^{-1} at a wavelength of 1080 km. This implies that weaker stratification over the plateau enhances the CISK development. The important role of reduced static stability on CISK can also be justified from Fig. 12. The dashed curve in Fig. 12 represents the growth rate calculated using the stronger stratification profile over Wuhan when all other parameters are kept constant. In this case, no instability occurs.

The increased moisture content in the plateau boundary layer also effectively contributes to the development of a CISK disturbance. For example, the monthly mean specific humidity in the layer between 600 and 530 mb is only 5.0 g kg^{-1} away from the plateau (at Wuhan) at 12 UTC in July but reaches as high as 7.2 g kg^{-1} over the central plateau. The increased moisture content over the plateau makes the CISK index, which is defined as the ratio of observed mean specific humidity in moist boundary layer to the model-predicted minimum threshold specific humidity (Wang, 1987b), quite comparable to that over a tropical ocean (Table 2). This means that the potential for CISK development in the plateau environment is comparable to that in a tropical oceanic environment. If the mean specific humidity in the boundary layer were the same as that over Wuhan, i.e., $\bar{q} = 5.0$ g kg^{-1}, and all the other conditions remained unchanged, the growth rate would then be given by the dotted curve in Fig. 12 and no unstable mode would be possible. It should be pointed out that, although the Coriolis parameter does not alter the minimum threshold specific humidity, it does significantly change the wavelength and the growth rate of the most unstable mode; the preferred wavelength is proportional to the inverse of the Coriolis parameter, while the maximum growth rate is proportional to the square root of the Coriolis parameter (Wang, 1987a,b). Thus the geographical location of the plateau is a major factor that favors the CISK development on meso-alpha scales.

In summary, the main features of the Tibetan plateau vortex seem to be captured qualitatively by the model CISK disturbance. Besides the presence of the conditionally unstable layer and the weak preexisting surface convergence, the development of a meso-alpha-scale CISK disturbance over the Tibetan Plateau can be ascribed primarily to 1) the small vertical heating extent in the upper troposphere, 2) the reduced background static stability, 3) the increased moisture content in the plateau boundary layer, and 4) the geographical location of the plateau. The numerical experiment carried out by Dell'Osso and Chen (1986) showed that the large-scale, horizontal inhomogeneous surface sensible heat flux does not directly contribute to the development of the plateau vortex, but rather has a damping effect. The sensible heating is not included in the present model, but the effect of sensible heating is implicitly considered in the temperature stratification and moisture content of the initial basic state. We note that the strong surface sensible heating may increase the conditional instability of the environment to cumulus convection and more importantly, may reduce the environmental static stability; hence it may significantly reduce the minimum threshold moisture content for CISK. As a result, the surface sensible heat flux makes an important indirect contribution to CISK development in the plateau environment.

5. Summary and conclusion

This paper studies the low-level cyclonic vortices that formed in situ over the main body of the Tibetan Plateau during the summer monsoon season. These are the major rain- and severe weather-producing systems over the plateau. Although the majority of the vortices remain on the plateau, some of them, under conditions of favorable large-scale circulation, may move eastward off the plateau, triggering the development of heavy rain vortex (the warm southwest vortex) on the lee side and influencing surface cyclogenesis along the downstream Meiyu front. Their dynamics involve complicated interactions between large-scale circulation and the thermal and dynamic effects of topography and between cumulus convection and meso-alpha-scale disturbances. Our dynamical understanding of these vortices has been rather limited because of the lack of observations over the plateau.

Using the GFDL limited-area mesoscale model, numerical simulations with and without latent heating were performed to assess the role of the convective latent heating and dynamic instability in the development of the plateau vortices. The model included an explicit formulation of moist convection and parameterized topographic effects of the high-resolution terrain. The results obtained from these experiments suggest that the vortex studied here is basically driven by latent heat release with the dynamic instability alone being unable to produce the observed vortex.

The monthly mean sounding in July at 1800 LST was used to indicate the convective instability of the environmental stratification in the air mass over the central plateau. Similarities exist between plateau vortices and tropical cyclones as far as the energy source and the conditionally unstable stratification of the environment are concerned. However, there are several significant differences. First, the planetary vorticity is much smaller over the tropics than over the plateau; secondly, the development and maintenance of tropical cyclones depend exclusively upon the heat and moisture transfer from the sea surface and the upper-ocean thermal energy (Emanuel, 1986), but the development of the plateau vortices is mainly sustained by the convective available potential energy in the atmosphere and exhibits significant diurnal variation. In addition, nonlinearity plays a nonnegligible part in the dynamics of intense tropical storms, whereas it may be reasonably neglected in the dynamics of plateau vortices because of their weaker circulation. These differences are of significance when one considers the applicability of CISK theory (Wang, 1987a).

CISK theory, in its essence, describes a linear instability resulting from the cooperative interaction between cumulus and larger-scale motions. Its applicability is not necessarily confined to maritime events. In fact, it is more appropriate to apply the theory to midlatitude or subtropical, small-amplitude systems that are driven by cumulus convective heating, such as the plateau vortices. However, since the water vapor content in the plateau boundary layer is only a little more than one-third of that in the boundary layer over a tropical ocean, the possibility of CISK development has not been clearly demonstrated.

The plateau vortices are characterized by a horizontal scale of several hundred kilometers and a weak circulation with wind speed of several meters per second, the typical scale for their relative vorticity is on the order of 10^{-5} s^{-1}, while the planetary vorticity is close to 10^{-4} s^{-1} over the plateau. The small Rossby number justifies the applicability of a quasi-geostrophic linear model.

A quasi-geostrophic continuous Ekman-CISK model with a basic environment similar to that actually observed over the summer Tibetan Plateau has been used to show that the CISK disturbances predicted by the model have a preferred scale, growth rate and vertical structure which are all qualitatively comparable to the observed features summarized in section 2. In particular, it was found that the minimum moisture content required by the most unstable CISK disturbance over the plateau is substantially smaller than that over a tropical ocean. This occurs because the condensational heat is released within a relatively shallow upper tropospheric layer and because the static stability of the midtropospheric layer over the plateau is lower than that of the surrounding region by about 40%, due to the strong surface sensible heat flux. This explains why an unstable CISK disturbance can be generated in an environment much drier than that over a tropical ocean. Furthermore, the moisture content in the plateau boundary layer is higher than that in the surrounding region by about 50%, due to the surface evaporation and monsoon moisture transport. These favorable factors, along with the geographical location (larger Coriolis parameter than in the tropics), further enhance the moist instability and shift the preferred horizontal scale to mesoscale. Because previously mentioned favorable factors mainly result from the influences of the elevated plateau topography, the mesoscale plateau vortices are unique products of the interactions between the plateau topography and the large-scale summer monsoon circulation and between the convective and subsynoptic-scale motions.

Acknowledgments. I would like to thank Drs. I. Orlanski and B. B. Ross for their comments and for their limited-area mesoscale model without which the numerical experiments in section 3 would be impossible. I would also like to thank Dr. N.-C. Lau and Prof. B.-Z. Zhu for reading and commenting on an early draft of the manuscript. I wish to express my appreciations to Mr. L. Polinsky for helping with the computer work, to Mr. Z.-A. Qian and Mr. W.-L. Li for discussing some observational aspects of this subject and for kindly providing weather maps. My thanks go to Mrs. Callan for typing the manuscript, and the GFDL drafting group for preparing the figures. This work was supported by NOAA/Princeton University Grant NA84EAD00057.

REFERENCES

Aubert, E. F., 1957: On the release of latent heat as a factor in large-scale atmospheric motion. *J. Meteor.*, **14,** 527–542.

Danard, M. B., 1964: On the influence of released latent heat on cyclone development. *J. Appl. Meteor.*, **3,** 27–37.

Dell'Osso, L. D., and S.-J. Chen, 1986: Numerical experiments on the genesis of vortices over the Qinghai-Tibet plateau. *Tellus,* **38A,** 236–250.

Charney, J. G., and A. Eliassen, 1964: On the growth of the hurricane depression. *J. Atmos. Sci.*, **21,** 68–75.

Emanuel, K. A., 1986: An air–sea interaction theory for tropical cyclones. Part I: Steady state maintenance. *J. Atmos. Sci.*, **43,** 586–604.

Gao, Y.-X., M.-C. Tang, S.-W. Luo, Z.-B. Shen and C. Li, 1981: Some aspects of recent research on the Qinghai-Xizang Plateau meteorology. *Bull. Amer. Meteor. Soc.*, **62,** 31–35.

Kuo, Y.-H., L. Cheng and R. A. Anthes, 1986: Mesoscale analyses of the Sichuan flood catastrophe, 11–15 July 1981. *Mon. Wea. Rev.*, **114,** 1984–2003.

Langer, R. E., 1960: *Boundary Problems in Differential Equations,* The University of Wisconsin Press, 324 pp.

Lu, J.-N., Z. A. Qian, F. M. Shan, Y. X. Cai and Y. C. Chen, 1984: Composite structure of summer Qinghai-Xizang Plateau low vortices, *Collected Works of QXPMEX (II),* 195–205, Science Press, Beijing. (in Chinese).

Luo, S.-W., 1979: Shear lines and vortices in the planetary boundary layer of Qinghai-Xizang Plateau, Chap. 9, *The Meteorology of Qinghai-Xizang Plateau,* by T. C. Yeh and Y. X. Gao et al., Eds., Science Press, Beijing 102–126 (in Chinese).

——, and Y.-P. Wang, 1984: Statistic analysis of weather systems over Qinghai-Xizang Plateau in May to August 1979, *Collected Works of QXPMEX(I),* Science Press, Beijing 269–278 (in Chinese).

Miyakoda, K., J. Smagorinsky, R. F. Stricker and G. D. Hembree, 1969: Experimental extended prediction with a nine-level hemispheric model. *Mon. Wea. Rev.*, **97,** 1–76.

Orlanski, I., and L. J. Polinsky, 1984: Predictability of mesoscale phenomena, mesoscale observations and very short-range forecasting, nowcasting II. *Proc., Second International Symposium on Nowcasting,* Norrkoping, Sweden, European Space Agency SP-208, 271–280.

Qian, Z.-A., F.-M. Shan, J.-N. Lu, Y.-X. Cai and Y.-C. Chen, 1984a: Statistics on Qinghai-Xizang Plateau vortices for summer 1979 and discussions on the climatological factors for the vortex genesis, *Collected Works of QXPMEX(II),* 182–194. Science Press, Beijing. (in Chinese).

——, S.-M. Zhang and F.-M. Shan, 1984b: Analysis of cumulus clouds over the plateau in summer 1979. *Collected Works of QXPMEX(I),* 243–257, Science Press, Beijing. (in Chinese).

Qin, H.-D., and X.-M. Cui, 1984: Radar echo analysis of a precipitating process of a low vortex near Naqu. *Collected Works of QXPMEX(II),* 206–214. Science Press, Beijing. (in Chinese).

——, H.-S. Zhou, J.-X. Liu, X.-R. Yang and Z. Qu, 1984: Statistic characteristics of radar echo of convective precipitation near Naqu over the Qinghai-Xizang Plateau. *Collected Works of QXPMEX(I),* 258–268. Science Press, Beijing. (in Chinese).

Ross, B. B., and I. Orlanski, 1982: The evolution of a cold front. Part I: Numerical simulation. *J. Atmos. Sci.*, **39,** 296–327.

Shapiro, L. J., 1986: The three-dimension structure of synoptic-scale disturbances over the tropical Atlantic. *Mon. Wea. Rev.*, **114,** 1876–1891.

Shen, Z.-B., 1979: The humidity field over Qinghai-Xizang Plateau and its neighborhood. *The Meteorology of the Qinghai-Xizang Plateau,* T. C. Yeh and Y. X. Gao et al., Eds., Science Press, Beijing. 39–48. (in Chinese).

Smagorinsky, J., 1960: On the dynamical prediction of large-scale condensation by numerical methods. *Geophys. Monogr.,* No. 5, Amer. Geophys. Union, 71–78.

Smith, P. J., P. M. Dare and S.-J. Lin, 1984: The impact of latent heat release on synoptical scale vertical motion and the development of extra-tropical cyclone system. *Mon. Wea. Rev.*, **112,** 2421–2430.

Tao, S.-Y., and Y.-H. Ding, 1981: Observational evidence of the influence of the Qinghai-Xizang (Tibet) Plateau on the occurrence of heavy rain and severe convective storms in China. *Bull. Amer. Meteor. Soc.*, **62,** 23–30.

Tracton, M. S., 1973: The role of cumulus convection in the development of extratropical cyclones. *Mon. Wea. Rev.*, **101,** 573–593.

Wang, B., 1987a: The nature of CISK in a generalized continuous model. *J. Atmos. Sci.*, **44,** 1411–1426.

——, 1987b: Another look at the CISK in polar oceanic air masses. *Tellus,* **39A,** 179–186.

——, and A. Barcilon, 1986: Moist stability of a baroclinic zonal flow with conditionally unstable stratification. *J. Atmos. Sci.*, **43,** 705–719.

——, and I. Orlanski, 1987: Study of a heavy rain vortex formed over the eastern flank of the Tibetan Plateau. *Mon. Wea. Rev.*, **115,** 1370–1393.

Yeh, T. C. (Duzheng Ye), 1979: Summary, Chap. 19, *The Meteorology of the Qinghai-Xizang Plateau,* T. C. Yeh and Y. X. Gao et al., Eds., Science Press, Beijing. pp. 267–275, (in Chinese).

——, 1981: Some characteristics of the summer circulation over the Qinghai-Xizang (Tibet) Plateau and its neighborhood. *Bull. Amer. Meteor. Soc.*, **62,** 14–19.